Erschienen in: Bioinspiration & Biomimetics. Institute of Physics Publishing (IOP). 2021, 16(1), 016012
https://doi.org/10.1088/1748-3190/abb86c

Artificial lateral line based relative state estimation between an upstream oscillating fin and a downstream robotic fish

Xingwen Zheng[1], Wei Wang[2,3], Liang Li[6,7,8] and Guangming Xie[1,4,5,*]

[1] State Key Laboratory for Turbulence and Complex Systems, Intelligent Biomimetic Design Lab, College of Engineering, Peking University, Beijing, 100871, People's Republic of China
[2] SENSEable City Laboratory, Massachusetts Institute of Technology, Cambridge, MA, 02139, United States of America
[3] Computer Science and Artificial Intelligence Lab (CSAIL), Massachusetts Institute of Technology, Cambridge, MA, 02139, United States of America
[4] Peng Cheng Laboratory, 518055 Shenzhen, People's Republic of China
[5] Institute of Ocean Research, Peking University, Beijing, 100871, People's Republic of China
[6] Department of Collective Behaviour, Max Planck Institute of Animal Behavior, Konstanz 78547, Germany
[7] Centre for the Advanced Study of Collective Behaviour, University of Konstanz, Konstanz 78547, Germany
[8] Department of Biology, University of Konstanz, Konstanz 78547, Germany
[*] Author to whom any correspondence should be addressed.

E-mail: xiegming@pku.edu.cn

Keywords: lateral line, robotic fish, underwater robot

Abstract

The lateral line enables fish to efficiently sense the surrounding environment, thus assisting flow-related fish behaviors. Inspired by this phenomenon, varieties of artificial lateral line systems (ALLSs) have been developed and applied to underwater robots. This article focuses on using the pressure sensor arrays based ALLS-measured hydrodynamic pressure variations (HPVs) for estimating the relative states between an upstream oscillating fin and a downstream robotic fish. The HPVs and relative states are measured in flume experiments in which the oscillating fin and the robotic fish have been locate with upstream-downstream formation in a flume. The relative states include the relative oscillating frequency, amplitude, and offset of the upstream oscillating fin to the downstream robotic fish, the relative vertical distance, the relative yaw angle, the relative pitch angle, and the relative roll angle between the upstream oscillating fin and the downstream robotic fish. Regression models between the ALLS-measured and the mentioned relative states are investigated, and regression models-based relative state estimations are conducted. Specifically, two criteria are proposed firstly to investigate not only the sensitivity of each pressure sensor to the variations of relative state but also the insufficiency and redundancy of the pressure sensors. And thus the pressure sensors used for regression analysis are determined. Then four typical regression methods, including random forest (RF) algorithm, support vector regression, back propagation neural network, and multiple linear regression method are used for establishing regression models between the ALLS-measured HPVs and the relative states. Then regression effects of the four methods are compared and discussed. Finally, the RF-based method, which has the best regression effect, is used to estimate the relative yaw angle and oscillating amplitude using the ALLS-measured HPVs and exhibits excellent estimation performance.

1. Introduction

The lateral line system is a sensory organ system existing in most fish and aquatic amphibians. It includes superficial neuromasts on the surface of the skin and canal neuromasts in subepidermal canals. Fish can detect the surrounding flow environment using its lateral line system. It has been demonstrated that the lateral line system assists fish in varieties of behaviors like rheotaxis, schooling, obstacle avoidance, and predation [1].

Recently, varieties of artificial lateral line systems (ALLSs) have been developed for their great potentials in improving the performance of underwater robots and surface vehicles, including remotely operated vehicle (ROV) [2], autonomous surface vehicle

(ASV) [3, 4], bio-inspired aquatic system [5], etc. The lateral line inspired researches cover from localization of dipole source [6–10], identification of flow characteristics [11–13], and applications on underwater robots [14–24]. Among the above-mentioned researches, investigating the applications of ALLS on underwater robots has been capturing an increasing attention. Kruusmaa *et al* have investigated rheotaxis, station holding, trajectory tracking, and swimming efficiency increasing of a fish-like robot with the aid of ALLS-measured flow variations [14]. Paley *et al* have studied speed evaluation and position control of a robotic fish based on an established flow field model and flow variations measured by the ALLS [15–17]. Tan *et al* have extensively explored ALLS based fixed and moving dipole source localisation using tank experiments and fluid dynamics simulations [6, 8]. Guo *et al* have implemented the estimation of angular acceleration and rectilinear speed of a robotic fish using the ALLS-measured HPVs. They have also realized wall following of the robotic fish by using the ALLS-measured flow variations to estimate the relative distance and angle to the wall [19, 20]. Kottapalli *et al* have investigated flow-related trajectory control of a robotic stingray and realized ALLS based obstacle avoidance and navigation of an underwater vehicle [18, 22, 23].

The above works have demonstrated the great application potentials of ALLS in underwater robots. However, the existing works have mainly studied the application of ALLS on one individual robot, rarely investigating an underwater robot group composed of two or more individuals with ALLS. On the other hand, the flow stimuli used in the above works typically include Kármán vortex street (KVS) behind a cylinder or cuboid, wave generated by a vibrating sphere, and uniform flow generated by well-controlled laboratory conditions. However, these flow stimuli have the limitations to emulate the hydrodynamic characteristics of natural flow stimuli like fish tail-generated reverse KVS, which has been rarely explored.

On the basis of the above analyses, our group has mainly focused on conducting the following investigations. For an upstream oscillating fin and a downstream robotic fish with leader–follower formation in a free stream, how the downstream robotic fish uses its onboard pressure sensor arrays based ALLS to detect a more natural flow stimulus, that is, the reverse KVS generated by the upstream oscillating fin, and then evaluates its relative states to its adjacent upstream oscillating fin [21, 25]. Specifically, The KVS generated by the upstream oscillating fin causes the hydrodynamic pressure variations (HPVs) in the flow field. Using ALLS, the downstream robotic fish can detect the pressure variations, thus detecting the reverse KVS indirectly. By extracting meaningful information from the ALLS readings, the qualitative relationships between the HPVs and the relative states including the relative oscillating frequency f, oscillating amplitude A, and oscillating offset ϕ of the upstream oscillating fin to the downstream robotic fish, the relative vertical distance d_{vertical}, the relative yaw angle α, the relative pitch angle β, and the relative roll angle γ between the upstream oscillating fin and the downstream robotic fish have been obtained [21].

Previous studies [21, 25] have mainly focused on the experiments, including experimental conditions, the experimental platform, the method of measuring the ALLS data, the visualisation of the ALLS data, and the explanation of data regularities. However, no models between the ALLS data and the relative states have been built. Thus the results cannot be directly used for realising the relative state estimation of the upstream oscillating fin and the downstream robotic fish. Whereas this article has mainly focused on the applications of the ALLS-measured flow variations in estimating the relative states, which is essential to flow-aided formation control of underwater robot group in the future. Specifically, we have focused on establishing a hydrodynamic model which refers to regression model linking the ALLS-measured HPVs of downstream robotic fish to the relative states.

However, only a few works [24, 26–28] have investigated modeling for hydrodynamic variations and it is always a challenge to precisely characterise the flow variations caused by the vortices. Potential flow theory has provided a promising approach for quantitatively describing the flow variations existing in fish tail-generated vortex wake [26] and surrounding fish body [24], thus establishing the above-mentioned regression model. However, the existing works have only focused on one individual fish or fish robot [24, 26]. The hydrodynamic variations modelings for two or more fish robots are quite different because it is extremely difficult to establish a model as reference, based on flow dynamics theories [29]. In this case, this article attempts to investigate a regression model between the ALLS data and the relative states using intelligent algorithms.

Before conducting the regression modeling, two criteria are proposed firstly for investigating the sensitivity of each pressure sensor to the variations of relative state, then the pressure sensors are sorted according to their sensitivities. Based on the order, the insufficiency and redundancy of the pressure sensors are analysed in detail. Then the reasonable number of pressure sensors used for regression analysis is determined. To the best of our knowledge, only a few works have investigated the sensitivity of sensors in ALLS [30]. [30] has focused on measuring the sensitivity of sensors to noise variance in the flow field, whereas we have focused on investigating the sensitivity of ALLS to the variations of relative state in this article. Besides, only a few works have analysed insufficiency and redundancy for sensor arrays based ALLS [31]. Such an investigation is helpful for critical for final robotic applications, especially for obtaining the

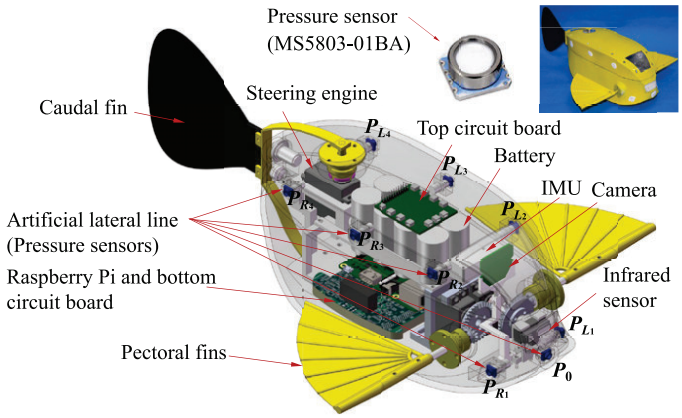

Figure 1. Boxfish-like robot with an ALLS. The pressure sensors used for forming the ALLS are named P_{L_m} and P_{R_m} $(m = 1, 2, 3, 4)$ (reused from [21] with permission of IOP Publishing).

best efficiency of the regression models using the least sensors, and thus decreasing the time of data processing when applying the regression model in online estimation.

Besides, because the regression model between the relative state and the flow variations around the robotic fish is unknown. We cannot determine which is the best method for investigating the above regression models. So four typical regression methods which have shown great performance in regression analysis of variables are used for establishing the regression model. The methods include random forest (RF) algorithm, support vector regression (SVR), back propagation neural network (BPNN), and multiple linear regression method (REG). And by comparing the regression effects of using the four methods in detail, the RF method has been determined as the best method. Finally, the estimations for two relative states, relative yaw angle and the oscillating amplitude of the upstream fin, have been conducted to verify the effectiveness of the RF method.

The contributions of this article can be concluded as follows:

1) Guiding the application of ALLS in local perception.

Particularly, this article investigates how to obtain the relative states between two an upstream vortices generator and a downstream robot with ALLS, by reversely solving the established regression models using the ALLS-measured HPVs.

2) Quantitatively investigating flow-aided multiple relative states sensing between two underwater robots.

We have investigated multiple relative states using ALLS-measured data measured in a large scope of experimental parameter space based on various intelligent algorithms. To the best of our knowledge, few lateral line inspired researches of underwater robots have investigated various states of the robot. And the experiments have mainly been conducted with a fairly limited experimental parameter space.

3) Analysing the sensitivity and insufficiency or redundancy of pressure sensors in ALLS.

We have defined the sensitivity of pressure sensor to the variations of relative state and then investigated insufficiency or redundancy of the number of the sensors used when extracting information from the ALLS-measured data, the above analyses have been seldom conducted before [30, 31].

The remainder of this article is organised as follows. Section 2 introduces the robotic fish with the ALLS. Section 3 describes the four methods, the criteria for measuring sensitivity of the pressure sensors-measured HPVs to the relative states, the importance measurement of the HPVs measured by each pressure sensor, and the evaluation of the regression model. Section 3 shows the pretreatment results of insufficiency and redundancy of the pressure sensors, the sample data and the regression results using the four methods. Section 4 discusses the work. Section 5 concludes this article with an outline of future work.

2. Experimental approach

2.1. The robotic fish with an artificial lateral line system

Figure 1 shows the configurations of the robotic fish used in the experiments. It is a boxfish-inspired robotic fish whose size (length × width × height) is about 40 cm × 14.1 cm × 13.2 cm. It consists of a sealed shell, a pair of pectoral fins, and a caudal fin. The electrical system, which includes a credit card-sized micro-computer called Raspberry Pi serving as the main processor, rechargeable batteries, steering engines, circuit boards, and multiple onboard sensors, is wrapped in the sealed shell. As shown in figure 2, the onboard sensors include an inertial measurement unit (IMU) serving for attitudes monitoring, a camera serving for environment capturing, an infrared sensor serving for obstacle avoidance, and a nine pressure sensors (MS5803-01BA, TE Connectivity Ltd) based ALLS serving for external HPVs measurement. More about the ALLS can be

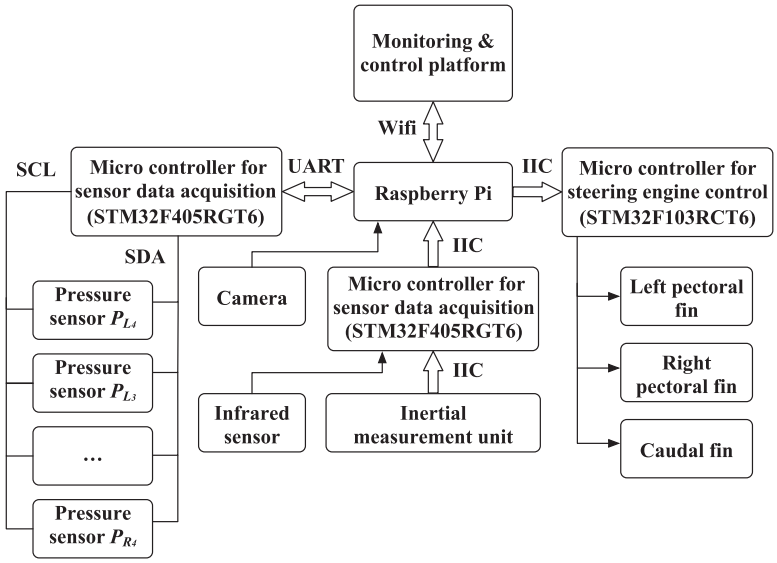

Figure 2. The diagrammatic sketch of the electrical system of the boxfish-like robot.

found in [21]. Multiple 32-bit micro controllers (STM32F405 and STM32F103) on the circuit boards serve the functions of sensor data acquisition and steering engine control. Through controlling the steering engines connected with the paired pectoral fins and the caudal fin with given oscillating amplitude, frequency, and offset parameters, the fins are able to generate propulsive forces which actuate the robotic fish for realizing multiple swimming patterns including rectilinear motion, turning motion, gliding motion, spiral motion, yawing motion, rolling motion, pitching motion, etc. Such multiple swimming patterns enable two adjacent robotic fish to form multiple relative positions and attitudes, as shown in figure 3.

2.2. Experimental description

As shown in figure 3, in the experiments, the pectoral fins and caudal fin of the downstream robotic fish have been removed. The two objects are located in a flume with a specific velocity of 0.175 m s^{-1}, with given relative states. The positions and attitudes of the two objects are controlled by controllable steering engines linked with them. Thus the relative states can be set, and there are 7 relative states including d_{vertical}, f, A, ϕ, α, β, and γ in total. For each relative state, we investigate p experimental parameters, and $p = 7$, 16, 6, 13, 19, 9, and 11 for d_{vertical}, A, f, ϕ, α, β, and γ, respectively. Details of the p experimental parameters mentioned above are defined in table 1. As we have mentioned in detail, this article mainly focuses on investigating the sensitivity of each pressure sensor, the insufficiency and redundancy of the pressure sensors, regression modeling, and model based relative state estimation using the measure experimental data, to avoid the repetition, more details about such a simplification, the control of relative states between the two adjacent objects, the experimental conditions, the experimental platform, and the method of measuring data can be found in [21]. The experimental scenes can be found in supplementary video (https://stacks.iop.org/JPBB/16/016012/mmedia). In the following part, we will use the ALLS-measured HPVs to estimate the above-mentioned relative states using the RF algorithm, BPNN, SVR method, and REG method.

2.3. Pretreatment of the data

Because of the hardware deficiency of the pressure sensors and the background noise in the environment, there exist significant fluctuations of the HPVs measured by the pressure sensors. In this case, we have smoothed the raw HPVs data using a Gaussian smoothing window function. Figure 4 shows the raw HPVs and the smoothed HPVs data. For the data in investigating d_{vertical}, α, β, and γ, the oscillating amplitude, frequency, and offset are set as 15°, 1 Hz, and 0. For the data in investigating ϕ, the above-mentioned parameters are 15°, 1 Hz, and 30°. For the data in investigating f, the above-mentioned parameters are 15°, 1.0 Hz, and 0. For the data in investigating A, the above-mentioned parameters are 30°, 1 Hz and 0. The sampling rate of the sensors is 50 Hz. In each recording, 250 samples of the HPVs are selected for forming the original sample set O used for regression model analysis. Taking the regression analysis for d_{vertical} for example, there are seven experimental parameters of d_{vertical}, varying from −45 mm to 45 mm, with an interval of 15 mm. For each experimental parameter, the HPVs recording is repeated five times. The final samples in the original sample set O for d_{vertical} have a size of $7 \times 5 \times 250 = 8750$.

2.4. Random forest for regression task

RF, proposed by Breiman L, is a decision-tree-based ensemble learning algorithm which can be

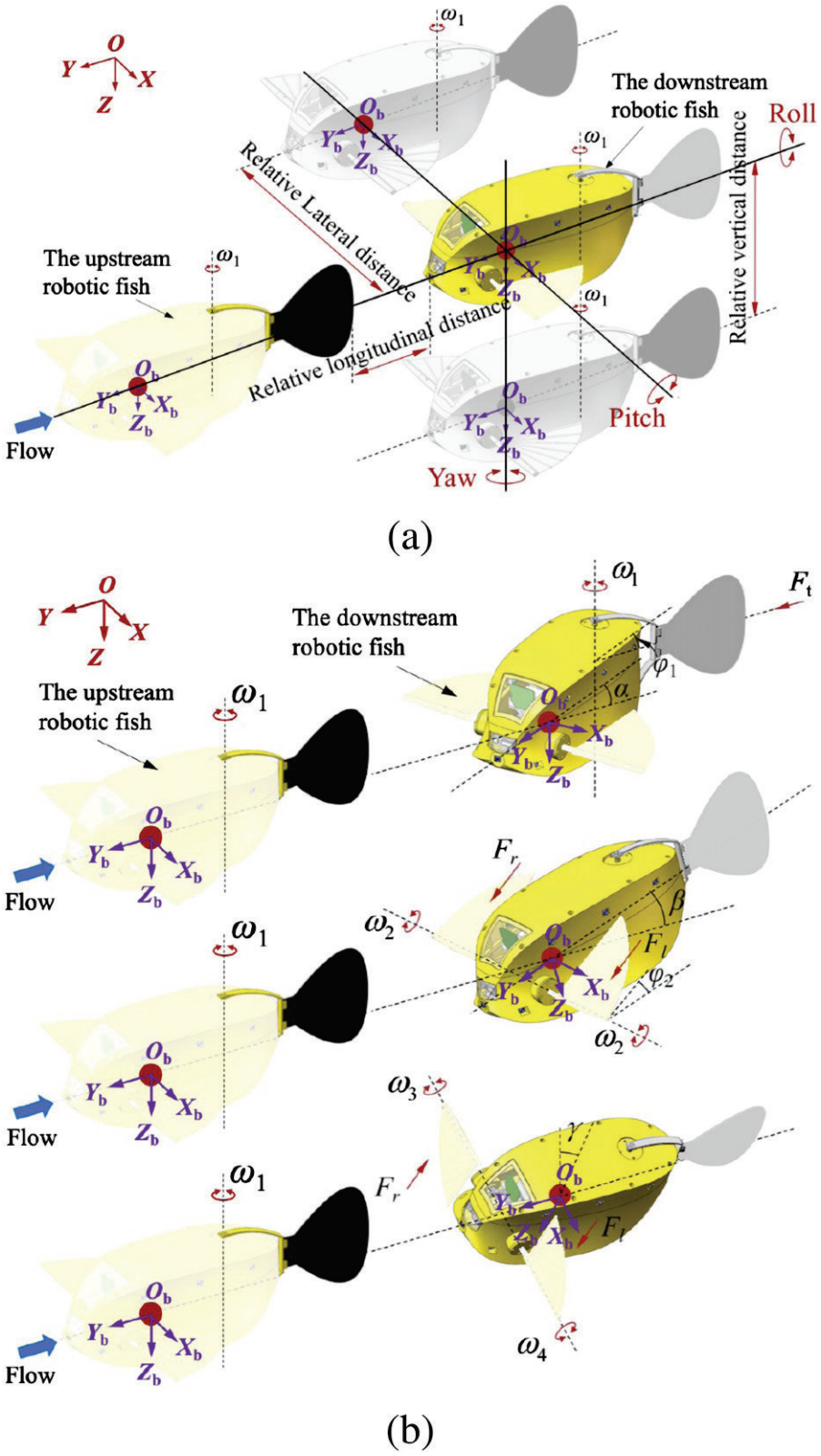

Figure 3. Relative positions and attitudes between an upstream oscillating fin and a downstream robotic fish with fins removed. (a) Relative positions between the upstream fin and downstream robotic fish and definition of the attitude motions. The red point indicates the center of mass of the robotic fish. The separations between the upstream fin and the downstream robotic fish along X, Y, and Z are defined as the relative lateral distance, the relative longitudinal distance, and the relative vertical distance, respectively. In the experiments, the longitudinal distance and lateral distance are set as 10 cm and 0. Except from the experiment of investigating relative vertical distance, the relative vertical distance is set as 0. (b) Relative attitudes between the upstream fin and downstream robotic fish. The relative attitudes include relative yaw angle α, relative pitch angle β, and relative roll angle γ. ω_1, ω_2, ω_3, and ω_4 indicate the angular velocities of the fins. φ_1 and φ_2 indicate the offsets of the fins. $OXYZ$ and $O_bX_bY_bZ_b$ indicate the global inertial coordinate system and the fish body-fixed coordinate system, respectively. F_t, F_l, and F_r indicate the propulsive force generated by the oscillating caudal fin, the left pectoral fin, and the right pectoral fin, respectively.

Table 1. Details of the p experimental parameters.

Items	p	Parameters
d_{vertical} (mm)	7	$-45, -30, -15, 0, 15, 30, 45$
A (degree)	16	$\{0, 2, 4, \ldots, 26, 28, 30\}$
f (Hz)	6	0.5, 0.6, 0.7, 0.8, 0.9, 1.0
ϕ (degree)	13	$\{30, -25, -20, \ldots, 20, 25, 30\}$
α (degree)	19	$\{-90, -80, -70, \ldots, 70, 80, 90\}$
β (degree)	9	$\{-20, -15, -10, \ldots, 10, 15, 20\}$
γ (degree)	11	$\{-50, -40, -30, \ldots, 30, 40, 50\}$

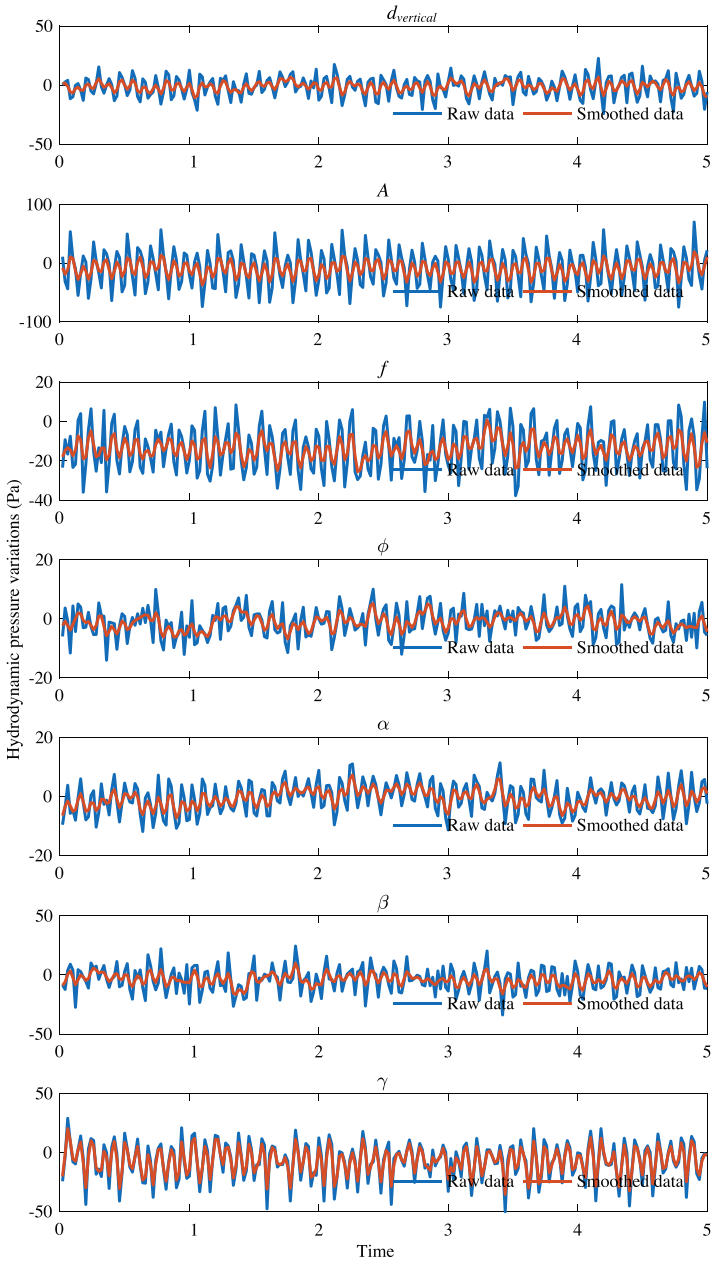

Figure 4. Raw data and smoothed HPVs measured by P_{L_1} in the experiments of investigating d_{vertical}, f, A, ϕ, α, β, and γ.

used for classification and regression [32]. In this article, RF is used for regression. A RF can be defined as $R = \{T_1(X), \ldots, T_N(X)\}$, consisting of N decision trees which are defined as $T_i (i = 1, \ldots, N)$. $X = \{X(1), \ldots, X(p)\}$ is a p-dimensional state vector. In a regression task, by importing X into the RF R, N estimated values $\hat{Y}_i (i = 1, \ldots, N)$ of Y are obtained, where $\hat{Y}_i$ indicates the estimated value of Y obtained by the tree T_i. $\hat{Y} = \frac{\hat{Y}_1 + \cdots + \hat{Y}_N}{N}$ is the estimated result of Y using multiple classifiers in the RF. The classifiers can learn and predict the results using the inputs. By importing a sample data

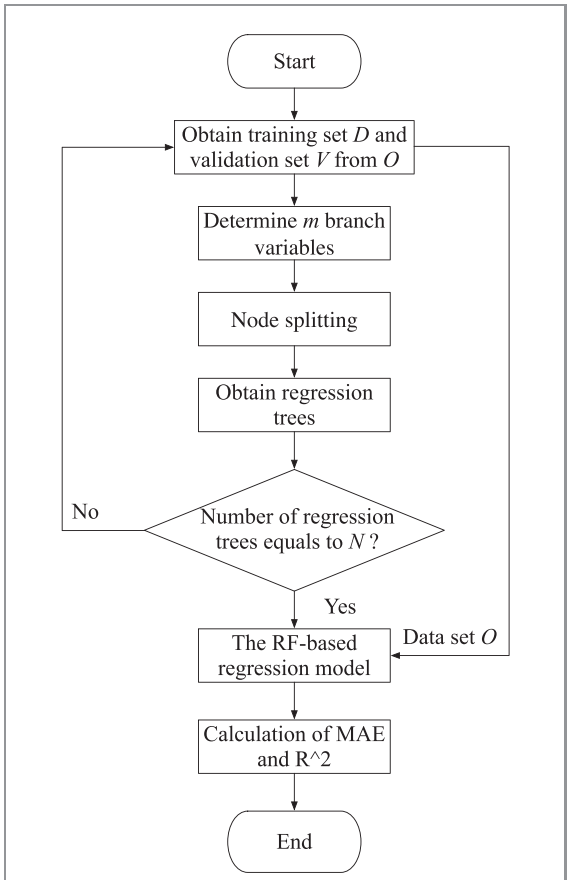

Figure 5. Algorithm flow of RF-based regression analysis.

set $D = \{(X_1, Y_1), \ldots, (X_n, Y_n)\}$ for training the RF model, a model which links $X_j (j = 1, \ldots, n)$ to Y_j can be obtained [33]. In this article, each sample in the original sample set consists of the HPVs measured by the nine pressure sensors of the ALLS and value of the relative state. Each sample can be defined as $\{S, P_0, P_{L_1}, P_{L_2}, P_{L_3}, P_{L_4}, P_{R_1}, P_{R_2}, P_{R_3}, P_{R_4}\}$, where S indicates value of the relative state, and other variables indicate the ALLS-measured HPVs. In this article, for each sample, the state vector X includes nine HPVs measured by the ALLS, and $X = \{P_0, P_{L_1}, P_{L_2}, P_{L_3}, P_{L_4}, P_{R_1}, P_{R_2}, P_{R_3}, P_{R_4}\}$. Y is the relative state S.

Figure 5 shows the flow of the RF for the regression task. It includes four steps described as follows [32, 33].

Step 1: obtain a bootstrap sample set of size n by randomly sampling with replacement from the original sample set O of size n, as a training set D of the established RF. The data samples which have not been sampled into the bootstrap sample set are called out-of-bag (OOB) samples and form a validation set V.

Step 2: randomly select m variables from M variables of the original sample set as branch variables at each node of each regression tree. Then determine the optimum splitting attributes according to the goodness of split criterion. In general, $m = M/3 \pm 1$. If $M < 3$, m is set as 1. In this article, the variables of the original sample indicate nine ALLS-measured HPVs, so $M = 1 \sim 9$.

Step 3: repeat Step 1 and 2 for N times, for obtaining N training sets and N validation sets. Then respectively establish an initial RF consisting of N regression trees $T_i (i = 1, \ldots, N)$ for the above training sets and validation sets.

Figure 6 shows the mean of squared residuals with N for $d_{\text{vertical}}, f, A, \phi, \alpha, \beta$, and γ. It can be seen that the mean of squared residuals gradually decreases with the increasing N, and it converges to the minimum when N exceeds 400. In this article, N is set as 500.

Step 4: calculate mean absolute error (MAE) and coefficient of determination (R^2) of the estimated results using the original sample set O.

2.5. Back propagation neural network (BPNN)

The artificial neural network has been widely used for modeling the relationship between the input signal and output signal. It has exhibited excellent performance in tasks of data classification, data speculation, and pattern identification [34]. BPNN is one of the neural networks which has the widest application. The information in a BPNN propagates forward, and the error propagates backward. The basic theory of BPNN is using gradient descent methods to make the mean square error between the actual output and the expected output least. For a BPNN, it consists of one input layer, one or more hidden layers, and one output layer. In each layer, there are several nodes [35]. In this article, the activation function of BPNN is the sigmoid function. And we have used L2 regularization (weight decay). A three-layer BPNN has been respectively structured for each experiment, as shown in figure 7. The BPNN has one input layer of which the number of nodes $p = 9$ and the nine HPVs in each sample are used as the node data. Besides, there is one output layer of which the number of nodes $q = 1$ and the relative state in each sample is used as the node data. Besides, there is one hidden layer of which the number of nodes m is determined as follows.

Figure 8 shows the training time and coefficient of determination R^2 with respect to the number of the nodes m in the hidden layer of BPNN for the estimation of β. reported R^2 score is from a training set. It can be seen that the training time increases with m, and R^2 varies little when the number of nodes exceeds 6. In this case, we have determined m as 6 for the estimation of β. Similarly, m has been determined as 11, 10, 9, 6, 13, 6, and 10 for the estimation of $d_{\text{vertical}}, A, f, \phi, \alpha, \beta$, and γ, respectively, according to figure 9.

As shown in figure 10, the training time increases with iterations of BPNN, and R^2 varies little when iterations exceeds 400. In this case, iterations of BPNN for α is determined as 400. reported R^2 score is from a training set. Figure 11 shows the coefficient of determination R^2 with iterations of BPNN for d_{vertical}, A, f, ϕ, α, β, and γ. Similarly, iterations of BPNN for $d_{\text{vertical}}, A, f, \phi, \alpha, \beta$, and γ are determined as 150, 250, 150, 200, 400, 150, and 300, respectively.

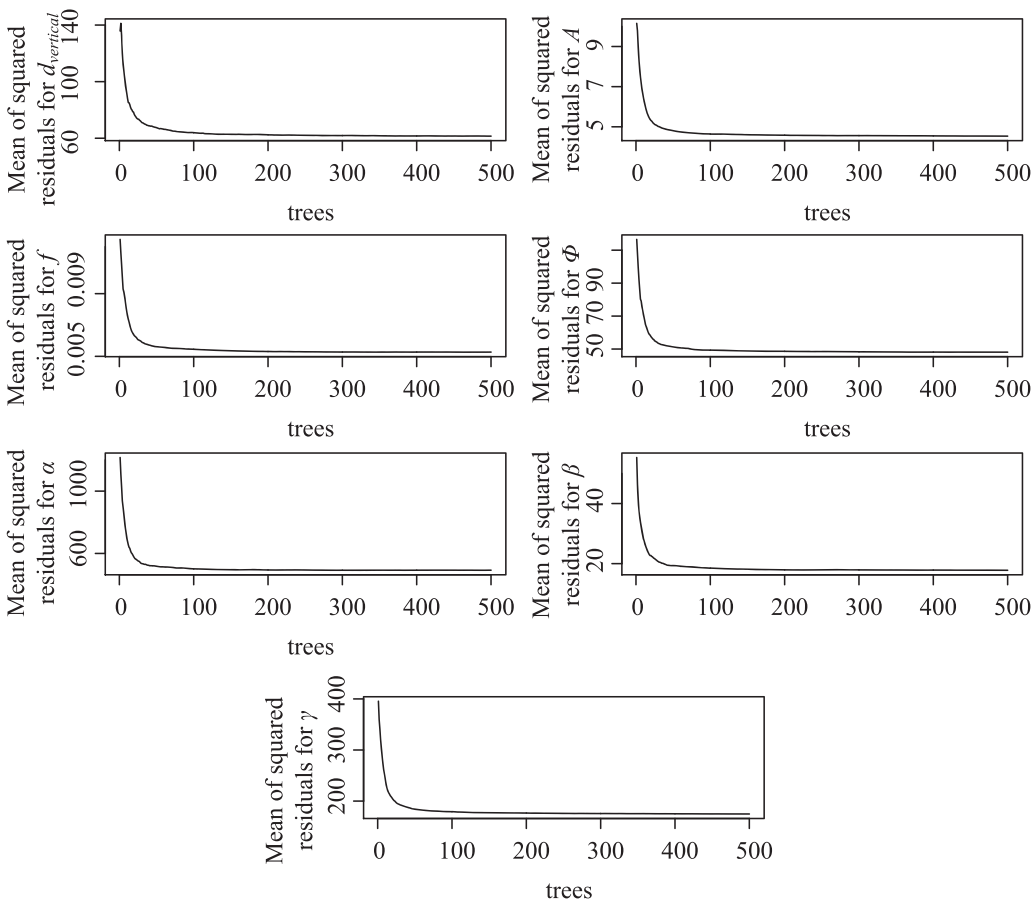

Figure 6. Mean of squared residuals with the number of regression trees (N) for d_{vertical}, f, A, ϕ, α, β, and γ in step 3 of RF based-regression task.

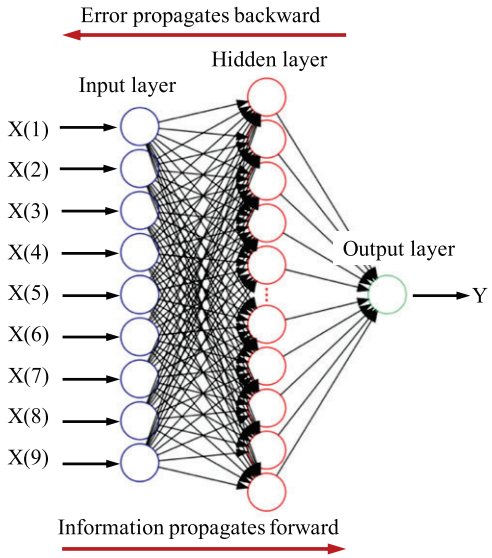

Figure 7. Topological structure of the BPNN.

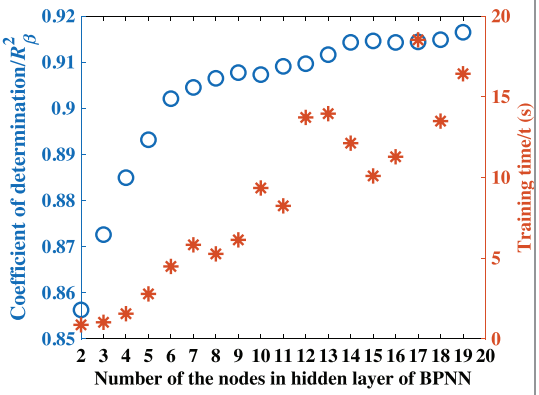

Figure 8. Training time (in $*$) and coefficient of determination R^2 (in o) with respect to number of the nodes in the hidden layer of BPNN for the estimation of β. The number of the variables used (M) equals 9. The iterations of BPNN equals 1000. The R^2 is obtained using training set.

2.6. Support vector regression (SVR) and multivariable linear regression (REG)

SVR is used to describe regression using support vector methods. It is developed from support vector machine (SVM) by introducing an alternative loss function [36]. In this article, SVR with eps-regression and radial basis function as the kernel is used to investigate the regression relationship between the relative state and the ALLS-measured HPVs.

REG refers to investigating a linear regressive relationship between a dependent variable and two or more independent variables. In this article, we establish a model for linking the ALLS-measured

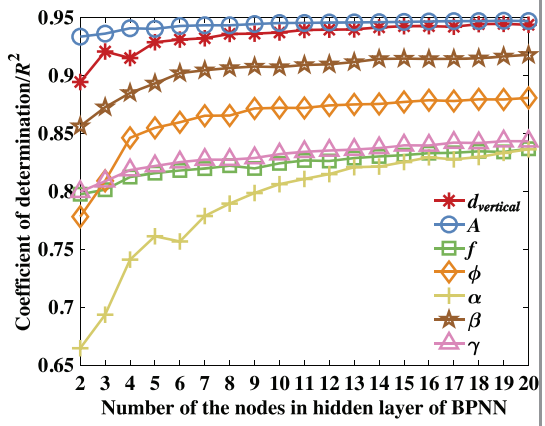

Figure 9. Coefficient of determination R^2 with m for all the experiments. Number of the variables used M equals 9. The R^2 is obtained using training set.

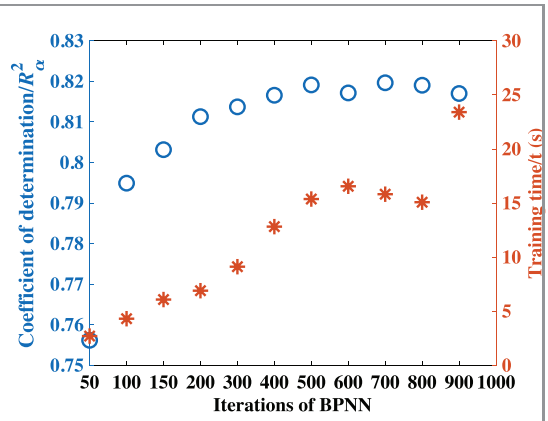

Figure 10. Training time (in *) and coefficient of determination R^2 (in o) with respect to iterations of BPNN for the estimation of α. The number of the variables used (M) equals 9. The R^2 is obtained using training set.

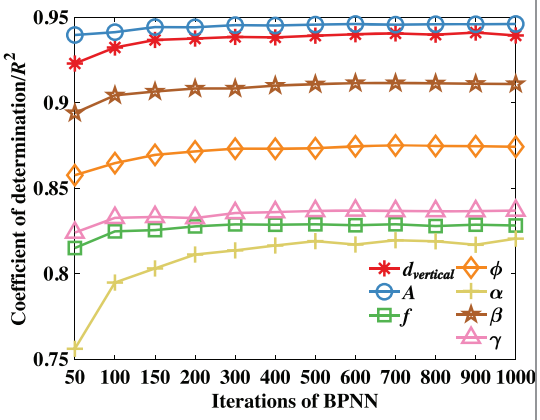

Figure 11. Coefficient of determination R^2 with iterations of BPNN for all the experiments. The number of the variables used (M) equals 9. The R^2 is obtained using training set.

HPVs to the relative states, as follows:

$$Y = a_0 + \sum a_k X(k) + \varepsilon \tag{1}$$

where Y is the relative state, a_0 is the intercept, a_k is the regression coefficient corresponding to the variable $X(k), k = 1, 2, \ldots, 9$, $X(k)$ indicates the HPVs measured by the nine pressure sensors, and ε is the residual error. F-test is conducted for verifying the rationality of the model. To be specific, the model has the rationality to explain the linear relationship between the dependent variable and the independent variables only when all of the regression coefficients do not equal to zero at the same time.

2.7. Sensitivity of the pressure sensors-measured HPVs to the relative states

In order to study the insufficiency and redundancy of the pressure sensors used for regression analysis, we have first proposed two criteria for measuring the sensitivity of the HPVs measured by the pressure sensors to the variations of relative states. The determination of the two criteria is described as follows.

Step 1: calculating the variations of the HPVs (ΔHPV) with the variations of the experimental parameters (ΔE) for each pressure sensor. The above experimental parameters include d_{vertical}, A, f, ϕ, α, β, and γ.

$$\Delta\overline{\text{HPV}_i(k)} = \overline{\text{HPV}_{i+1}(k)} - \overline{\text{HPV}_i(k)} \tag{2}$$

where $i = 1, 2, \ldots, p-1$. p is the number of the experimental parameters, and $p = 7$, 16, 6, 13, 19, 9, and 11 for d_{vertical}, A, f, ϕ, α, β, and γ, respectively. $\overline{\text{HPV}_i(k)}$ indicates the mean HPVs of 500 samples in the ith experimental parameter for $X(k)$.

Step 2: calculating the difference $\Delta\overline{\text{HPV}_i(k)}$ between the maximum and the minimum of $\overline{\text{HPV}_i(k)}$.

$$mm\overline{\text{HPV}_i(k)} = \max \overline{\text{HPV}_i(k)} - \min \overline{\text{HPV}_i(k)} \tag{3}$$

Step 3: nondimensionalize the $\Delta\overline{\text{HPV}_i(k)}$.

$$\Delta\overline{\text{HPV}_i(k)}' = \frac{\Delta\overline{\text{HPV}_i(k)}}{mm\overline{\text{HPV}_i(k)}} \tag{4}$$

Step 4: calculate the mean of $\Delta\overline{\text{HPV}_i(k)}'$ and the mean of $\Delta\overline{\text{HPV}_i(k)}$.

$$C_{k_1} = \frac{\sum_{i=1}^{p-1} \Delta\overline{\text{HPV}_i(k)}'}{p-1} \tag{5}$$

$$C_{k_2} = \frac{\sum_{i=1}^{p-1} \Delta\overline{\text{HPV}_i(k)}}{p-1} \tag{6}$$

C_{k_1} and C_{k_2} are the two criteria that are respectively used for measuring the sensitivity of $X(k)$ to the variations of relative state. In the experiments, fish head of the downstream robot directly faces to the vortex wake generated by the upstream oscillating caudal fin, so the vortex wake has a more significant effect on the fish head. And thus, the HPVs measured by the pressure sensors around the fish head are significantly bigger than HPVs measured by

Table 2. C_{k_1} of each pressure sensor in each experiment.

	d_{vertical}	A	f	ϕ	α	β	γ
P_0	0.3165	0.0667	0.2000	0.1633	0.1691	0.2446	0.4535
P_{L_1}	0.3117	0.1109	0.2000	0.1340	0.1268	0.2586	0.1495
P_{L_2}	0.1672	0.2608	0.4971	0.2757	0.1420	0.1713	0.1205
P_{L_3}	0.2676	0.3224	0.3555	0.2394	0.1336	0.2439	0.1000
P_{L_4}	0.4260	0.3172	0.3354	0.2143	0.1113	0.3339	0.2280
P_{R_1}	0.3280	0.0968	0.2025	0.1427	0.1205	0.2199	0.1708
P_{R_2}	0.1723	0.2442	0.5251	0.2713	0.1276	0.1606	0.1167
P_{R_3}	0.3130	0.3174	0.4818	0.2009	0.1346	0.3175	0.1000
P_{R_4}	0.2750	0.3012	0.5028	0.2162	0.1030	0.2462	0.1009

Table 3. C_{k_2} of each pressure sensor in each experiment.

	d_{vertical}	A	f	ϕ	α	β	γ
P_0	11.3143	3.4602	2.5864	3.8769	5.2647	6.9166	0.9537
P_{L_1}	2.3996	1.6968	1.7521	2.4489	4.4564	3.0227	1.6151
P_{L_2}	1.4778	1.3393	1.1334	1.1984	2.0292	1.6177	1.0072
P_{L_3}	0.6341	1.2951	0.8205	1.3811	1.1658	1.6542	0.5840
P_{L_4}	1.0560	1.4444	0.4281	1.1442	1.2445	1.6735	0.2736
P_{R_1}	2.2620	1.4399	1.5111	2.1011	4.1315	2.9065	1.4136
P_{R_2}	1.7180	1.2739	0.8769	1.1659	2.0737	1.9250	0.9149
P_{R_3}	0.7541	1.3676	0.6749	1.1011	1.2411	1.0540	0.4223
P_{R_4}	0.6398	1.2407	0.9156	0.9262	1.2121	1.5360	0.1482

Table 4. Sorting the order of the HPVs measured by the pressure sensors according to C_{k_1} (from biggest to smallest).

Experiments	Order
d_{vertical}	$P_{L_4}, P_{R_1}, P_0, P_{R_3}, P_{L_1}, P_{R_4}, P_{L_3}, P_{R_2}, P_{L_2}$
A	$P_{L_3}, P_{R_3}, P_{L_4}, P_{R_4}, P_{L_2}, P_{R_2}, P_{L_1}, P_{R_1}, P_0$
f	$P_{R_2}, P_{R_4}, P_{L_2}, P_{R_3}, P_{L_3}, P_{L_4}, P_{R_1}, P_0, P_{L_1}$
ϕ	$P_{L_2}, P_{R_2}, P_{L_3}, P_{R_4}, P_{L_4}, P_{R_3}, P_0, P_{R_1}, P_{L_1}$
α	$P_0, P_{L_2}, P_{R_3}, P_{L_3}, P_{R_2}, P_{L_1}, P_{R_1}, P_{L_4}, P_{R_4}$
β	$P_{L_4}, P_{R_3}, P_{L_1}, P_{R_4}, P_0, P_{L_3}, P_{R_1}, P_{L_2}, P_{R_2}$
Γ	$P_0, P_{L_4}, P_{R_1}, P_{L_1}, P_{L_2}, P_{R_2}, P_{R_4}, P_{L_3}, P_{R_3}$

pressure sensors at the posterior. In order to ensure the comparability of different pressure sensors, we have nondimensionalized the $\Delta\overline{\text{HPV}_i(k)}$ and then calculate C_{k_1}. On the other hand, we have also calculated calculate C_{k_2} using the $\Delta\overline{\text{HPV}_i(k)}$, which has not been nondimensionalized.

Table 2 and 3 show C_{k_1} and C_{k_2} of each pressure sensor in each experiments. A bigger value of C_{k_1} or C_{k_2} means a bigger sensitivity. We have sorted the HPVs measured by the pressure sensors from biggest to smallest according to C_{k_1} and C_{k_2}, respectively. Table 4 and 5 show the order of the HPVs measured by the pressure sensors from biggest to smallest based on the value of C_{k_1} and C_{k_2}. It can be seen that there are significant differences between the two orders of the HPVs.

Then we have successively selected the first (M) sensors in the information-criterion-ordered lists, for establishing the regression model and thus ensuring that the pressure sensors used are not redundant or insufficient. For example, when $M = 3$, we used the first M pressure sensors for regression analysis. The comparisons of regression results corresponding to C_{k_1} and C_{k_2} have been conducted in the following part.

2.8. Importance measurement of the HPVs measured by each pressure sensor

Importance measurement is conducted for evaluating the importance of the HPV measured by a pressure sensor (variable $X(k)(k = 1, \ldots, p)$ in the state vector X) to the relative state in RF-based analysis. The detailed processes of conducting importance measurement are as follows.

Step 1: obtain an initial RF model, including N trees. Then respectively calculate the mean-square error (MSE) of the estimated results using N OOB samples. And the obtained MSEs can be defined as $\text{MSE}_i(i = 1, \ldots, N)$, taking the form as

$$\text{MSE}_i = \frac{\sum_{j=1}^{n} \left(\hat{Y}_i(j) - Y_i(j)\right)^2}{n} \tag{7}$$

where $\hat{Y}_i(j)$ and $Y_i(j)$ indicate the jth estimated value and actual relative state value in the ith OOB sample, respectively.

Table 5. Sorting the order of the HPVs measured by the pressure sensors according to C_{k_2} (from biggest to smallest).

Experiments	Order
d_{vertical}	$P_0, P_{L_1}, P_{R_1}, P_{R_2}, P_{L_2}, P_{L_4}, P_{R_3}, P_{R_4}, P_{L_3}$
A	$P_0, P_{L_1}, P_{L_4}, P_{R_1}, P_{R_3}, P_{L_2}, P_{L_3}, P_{R_2}, P_{R_4}$
F	$P_0, P_{L_1}, P_{R_1}, P_{L_2}, P_{R_4}, P_{R_2}, P_{L_3}, P_{R_3}, P_{L_4}$
Φ	$P_0, P_{L_1}, P_{R_1}, P_{L_3}, P_{L_2}, P_{R_2}, P_{L_4}, P_{R_3}, P_{R_4}$
A	$P_0, P_{L_1}, P_{R_1}, P_{R_2}, P_{L_2}, P_{L_4}, P_{R_3}, P_{R_4}, P_{L_3}$
B	$P_0, P_{L_1}, P_{R_1}, P_{R_2}, P_{L_4}, P_{L_3}, P_{L_2}, P_{R_4}, P_{R_3}$
Γ	$P_{L_1}, P_{R_1}, P_{L_2}, P_0, P_{R_2}, P_{L_3}, P_{R_3}, P_{L_4}, P_{R_4}$

Step 2: randomly permute $X(k)(k = 1, \ldots, p)$ of the state vector X in the OOB samples, for obtaining new OOB samples. Then calculate the $\text{MSE}_i(k)(i = 1, \ldots, N; k = 1, \ldots, p)$ of the estimated results using the new OOB samples. Based on the above processes, an MSE matrix can be obtained, taking the form as

$$\begin{pmatrix} \text{MSE}_1(1) & \text{MSE}_2(1) & \ldots & \text{MSE}_N(1) \\ \text{MSE}_1(2) & \text{MSE}_2(2) & \ldots & \text{MSE}_N(2) \\ \vdots & \vdots & \vdots & \\ \text{MSE}_1(p) & \text{MSE}_2(p) & \ldots & \text{MSE}_N(p) \end{pmatrix} \tag{8}$$

Step 3: calculate the difference between elements in $[\text{MSE}_1, \ldots, \text{MSE}_N]^{\text{T}}$ and $[\text{MSE}_i(1), \ldots, \text{MSE}_i(p)]^{\text{T}}$, and the difference can be defined as

$$\Delta\text{MSE}_i(k) = \text{MSE}_i - \text{MSE}_i(k) \tag{9}$$

where $i = 1, \ldots, N$, and $k = 1, \ldots, p$.

Step 4: calculate the importance of variable $X(k)(k = 1, \ldots, p)$. The importance value I_k is defined as

$$I_k = \frac{\sum_{i=1}^{N} \Delta\text{MSE}_i(k)}{N \cdot \text{SE}_k} \tag{10}$$

where SE_k is the standard error of $\Delta\text{MSE}_i(k)(i = 1, \ldots, N)$, taking the form as

$$\text{SE}_k = \sqrt{\frac{\sum_{i=1}^{N} (\Delta\text{MSE}_i(k) - \overline{\text{MSE}_k})^2}{N}} \tag{11}$$

where $\overline{\text{MSE}_k}$ is the mean of $\Delta\text{MSE}_i(k)(i = 1, \ldots, N)$. A bigger I_k indicates that $X(k)$ is more important in the regression model.

2.9. Evaluation of the regression model

Mean absolute error (MAE) and coefficient of determination (R^2) are used for evaluating the accuracy of the above-trained regression model. Smaller MAE and bigger R^2 indicate a more accurate model.

$$\text{MAE} = \frac{\sum_{j=1}^{n} |\hat{y}_j - y_j|}{n} \tag{12}$$

$$R^2 = 1 - \frac{\sum_{j=1}^{n} (y_j - \hat{y}_j)^2}{\sum_{j=1}^{n} (y_j - \bar{y})^2} \tag{13}$$

where $\hat{y}_i$ and y_i indicates the estimated value and actual relative state value in the ith sample. $\bar{y}$ indicates the mean of $y_j(j = 1, \ldots, n)$.

3. Results

3.1. Insufficiency and redundancy of the pressure sensors

In the investigation of insufficiency and redundancy of the pressure sensors, we aim to find the least number of pressure sensors, with which the accuracy of estimation is big enough. Besides, when the number used for estimation increases, the accuracy of estimation has not increased much more. Such a characteristic means that the pressure sensors are neither insufficient nor redundant. Figure 12 shows the mean absolute error MAE with the used number of pressure sensors (M). It can be seen that MAE decreases with the increasing M as a whole. Figure 13 shows the coefficient of determination R^2 with the used number of sensors. $R^2_{d_{\text{vertical}}}$, R^2_A, R^2_f, R^2_A, R^2_ϕ, R^2_α, R^2_β, and R^2_γ indicates R^2 in the experiments of investigating d_{vertical}, A, f, ϕ, α, β, and γ. It can be seen that R^2 increases with the number of M as a whole in each experiment when using the four methods. Comparing the MAE and R^2 obtained based on the order of HPVs sorted by C_{k_1} and C_{k_2}, it can be seen that regression models obtained according to order of HPVs sorted by C_{k_2} have better effects. From this perspective, C_{k_2} is more reasonable for measuring the sensitivity of the HPVs measured by pressure sensors to the variations of relative states. In the following part, we mainly focus on the results corresponding to C_{k_2}.

Take the experiment of investigating d_{vertical} for example, a more careful inspection reveals that R^2 and MAE vary little when M exceeds 4. This characteristic demonstrates that 4 pressure sensors which specifically refer to P_0, P_{L_1}, P_{R_1}, and P_{R_2} here are enough for regression analysis. In other words, five or more pressure sensors are redundant. In this way, the reasonable numbers (defined as M_r) of pressure sensors used for regression analyses of d_{vertical}, A, f, ϕ, α, β, and γ are determined as 4, 1, 3, 4, 7, 4, and 5, respectively.

3.2. Regression results using the four methods

In order to have a fair comparison of all of the regression methods, similar cross-validations have been conducted when we conducting regression analyses. In each experiment, R^2s obtained by the RF algorithm

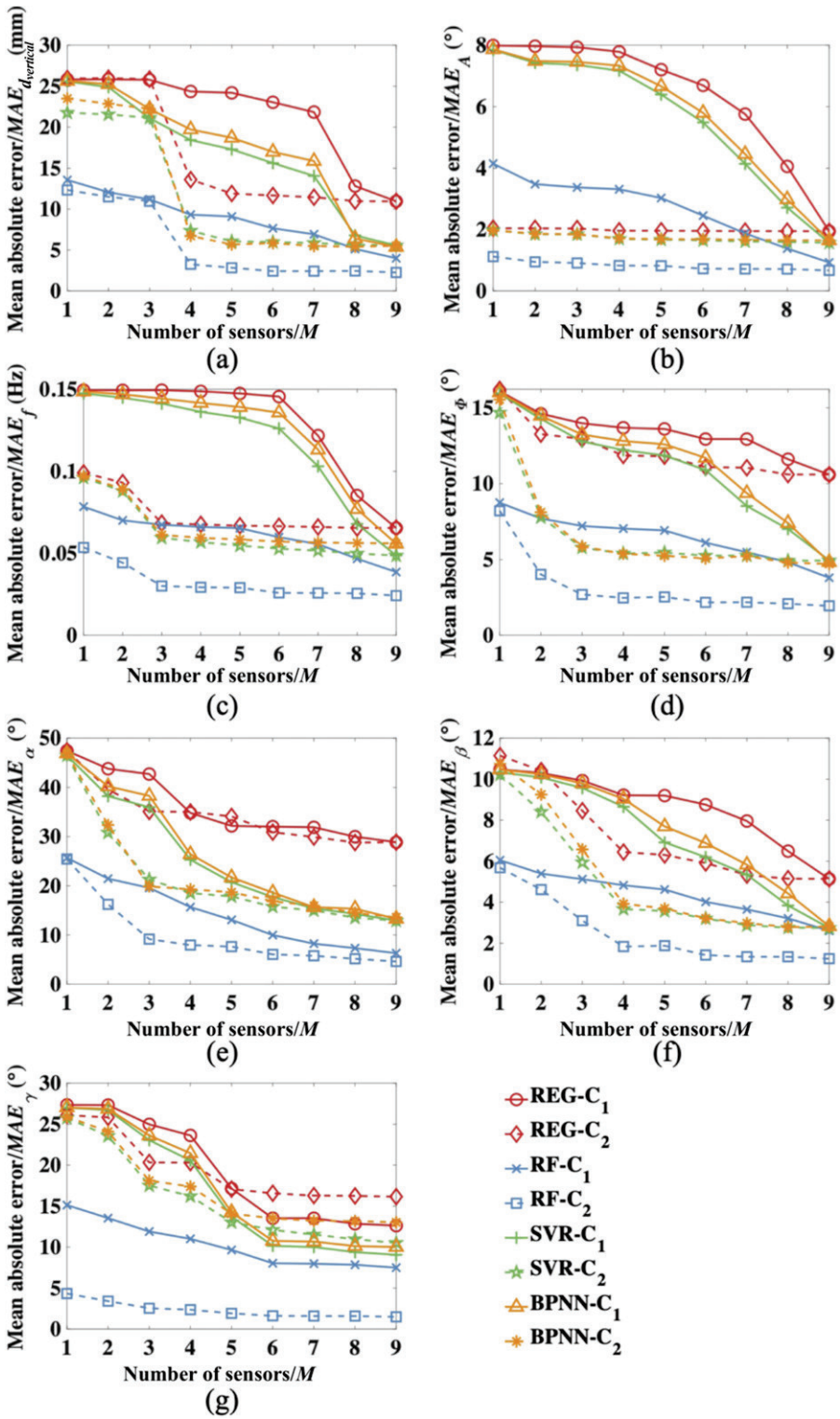

Figure 12. MAE with the varied number of sensors (M) when using RF algorithm, BPNN, SVR method, and REG method. Take REG-C_1 for example, it refers to the result obtained by the REG method based on the order of the pressure sensor sorted by C_{k_1}. The MAE is obtained using training set.

is bigger than R^2s obtained by BPNN, REG, and SVR. A further inspection has revealed that R^2 obtained by RF has the best performance though M is small. Based on the above analyses, we can conclude that the RF algorithm has better regression effects than the other three methods. Besides, R^2 obtained by the RF algorithm varies smoothly whereas the R^2 obtained by the other three methods have more significant variations with M. Such a characteristic demonstrates that RF has better noise-resistibility. On the above analyses, a conclusion can be obtained that RF algorithm has the best regression effect.

Figure 14 shows the estimated and actual relative states obtained by the RF algorithm with $M_r = 4, 1,$

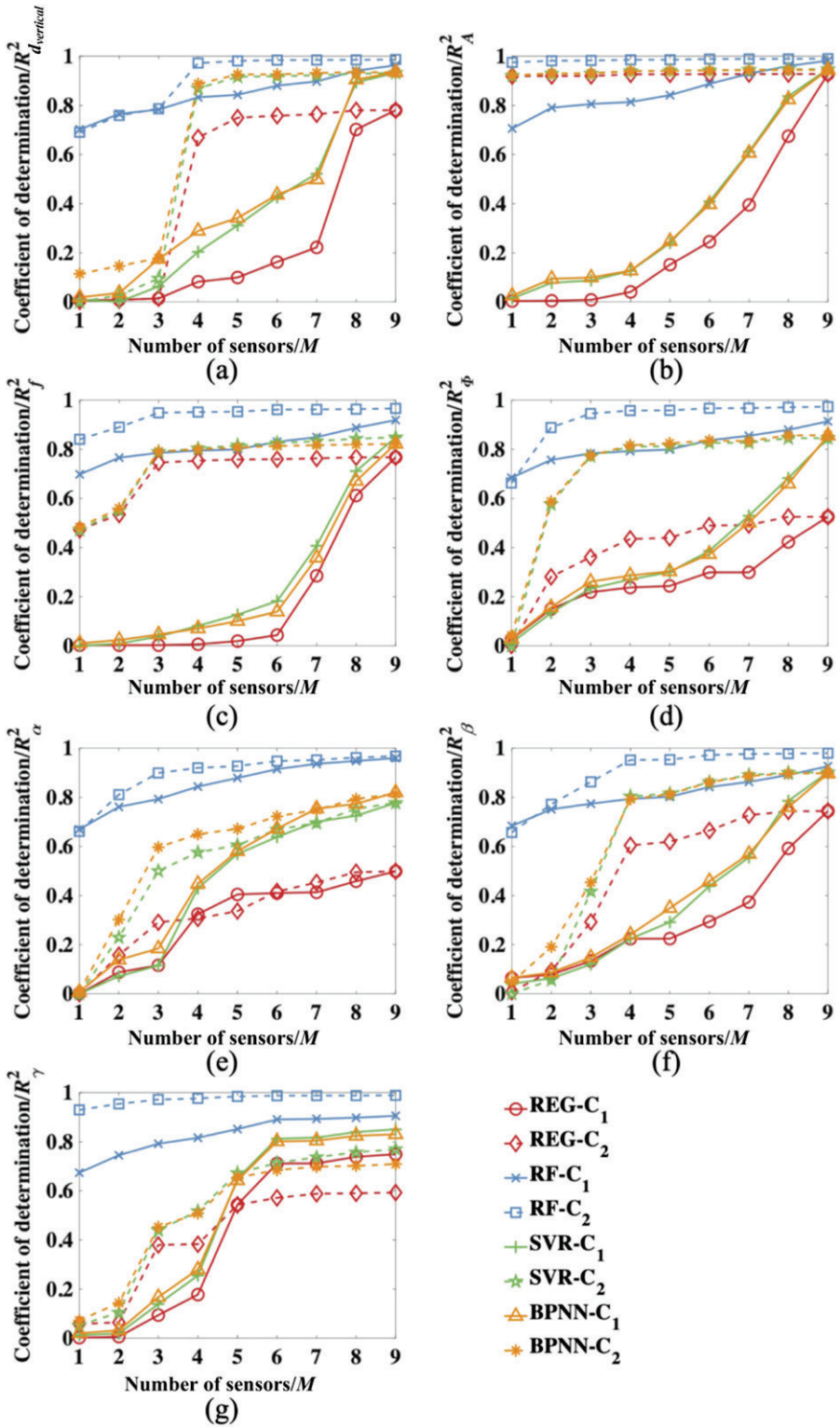

Figure 13. Coefficient of determination (R^2) with the varied number of sensors (M) when using RF algorithm, BPNN, SVR method, and REG method. The R^2 is obtained using training set.

3, 4, 7, 4, and 5 for the experiment of d_{vertical}, A, f, ϕ, α, β, and γ, respectively. On the whole, it can be seen that the established RF based regression models have good performances for describing the relative states. Specifically, the combination of the R^2, MAE, and M_r corresponding to the best regression effect is defined as (R^2, MAE, M), which refers to (0.972, 3.250 mm, 4), (0.975, 1.119°, 1), (0.949, 0.030 Hz, 3), (0.958, 2.467°, 4), (0.952, 5.778°, 7), (0.952, 1.836°, 4), and (0.985, 1.915°, 5) for the experiment of d_{vertical}, A, f, ϕ, α, β, and γ, respectively.

Figure 15 shows the order of the variables $X(k)$ sorted by the importance I_k. A bigger I_k indicates that the variable $X(k)$ is more important to the

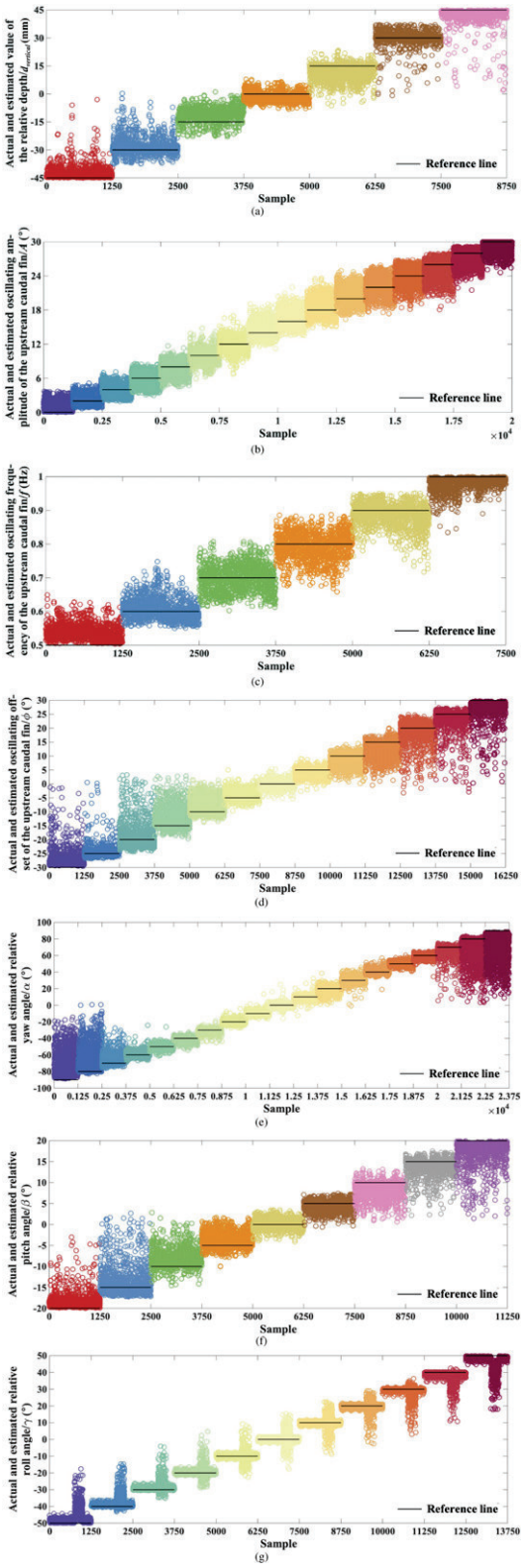

Figure 14. The actual relative states and estimated values obtained by the RF algorithm based regression model. In each subfigure, the different colors indicate the estimations for specific values of the relative states.

relative state in the RF-based regression analysis. The combinations of the M_r most important variables for d_{vertical}, A, f, ϕ, α, β, and γ are (P_0, P_{R_2}, P_{L_2}, P_{L_1}), (P_0), (P_{R_1}, P_{L_1}, P_0), (P_{L_1}, P_{R_1}, P_0, P_{L_3}), (P_{R_1}, P_{R_2}, P_{L_1}, P_{R_4}, P_0, P_{L_2}, P_{L_4}), (P_0, P_{R_2}, P_{L_3}, P_{L_2}), and (P_{R_2}, P_{L_2}, P_{L_1}, P_{R_1}, P_{L_3}), respectively. That is to say, we have determined the M_r pressure sensors used for estimation. A further investigation has revealed that M_r pressure sensors in the above combinations are almost the first M_r pressure sensors in table 5 for each experiment. Such a characteristic demonstrates also proves that it is reasonable for sorting the pressure sensors according to C_{k_2} because the first M_r pressure sensors in table 5 happen to be the most important in the regression analyses. Besides, there exist differences between concrete orders of pressure sensors in the above combinations and table 5. Such a characteristic demonstrates that the sensitivity of the pressure sensors-measured HPVs to the relative states is not the same thing as the importance of the HPVs.

3.3. Random forest algorithm based relative yaw angle estimation and oscillating amplitude estimation

The above work has shown that RF method has the best regression effect. In this part, we validate the effectiveness of RF method in relative state estimation. Considering that the number of the investigated experimental parameters, d_{vertical}, A, f, ϕ, α, β, and γ, is 7, 16, 6, 13, 19, 9, and 11, respectively. Here, we select the experiments of investigating A and α for validation works because more experimental parameters have been considered. Specifically, 80% data in the data set O form a training set for training the RF-based models which are different from the models in the section 4.2, and the remaining 20% data form a test set, for validating the effect of the RF-based models in estimating the relative yaw angle and the oscillating amplitude. Figure 16 shows the results of RF-based oscillating amplitude and relative yaw angle estimation. R^2 and MAE of the regression model for oscillating amplitude estimation is 0.975 and 1.091°, respectively. And the MAEs of the oscillating amplitude obtained by test set are 2.171°, 3.163°, and 3.211° for $A = 4°, 14°, 28°$, respectively. R^2 and MAE of the regression model for the relative yaw angle is 0.956 and 5.513°, respectively. And the MAEs of the relative yaw angle obtained by test set are 9.284°, 7.506°, 7.694°, and 45.435° for $\alpha = -60°, -30°, 30°, 60°$, respectively. It can be seen that the regression model has a bad performance when the relative yaw angle is big enough. However, it performs well when the relative yaw angle is small. The estimation errors may mainly result from the low noise-signal ratio of the HPVs measured by the pressure sensors. Though the pretreatment of the HPVs has been conducted, the hardware deficiency of the pressure sensors has reduced the estimation accuracy. In this case, improving the ALLS is necessary and urgent for improving the data quality. Besides, further data pretreatment by fusing ALLS data and IMU data may also provide a potential way for improving the estimation accuracy. The above-mentioned will

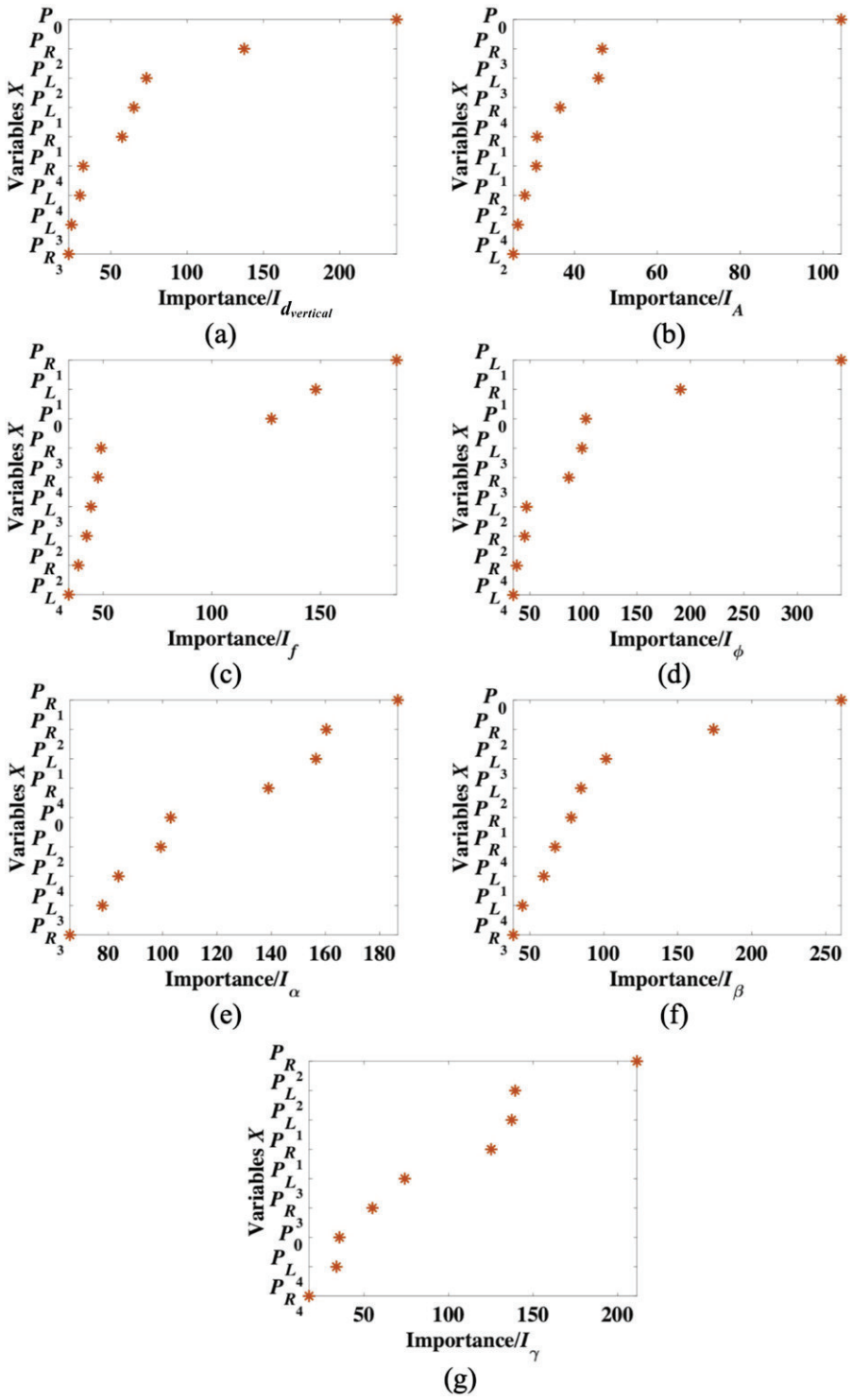

Figure 15. Variables $X(k)$ order sorted by the importance I_k.

be conducted in the following researches on multiple adjacent freely-swimming robotic fish.

4. Discussions

4.1. Why have we focused on close-range sensing?

As shown in figure 17, the relationship between the HPV and the relative lateral distance varies with the different relative longitudinal distances. There is a common qualitative regularity existing in the HPV curves under a short-range relative longitudinal distance. However, when the relative longitudinal distance exceeds a specific value, the above-mentioned qualitative regularity disappears. This may be because the vortex wake generated by the upstream oscillating fin scatters and disappears with the increasing propagation distance. To acquire significant regularities between the HPVs and the relative states, we have mainly focused on close-range sensing (local sensing), and the relative longitudinal distance of the upstream

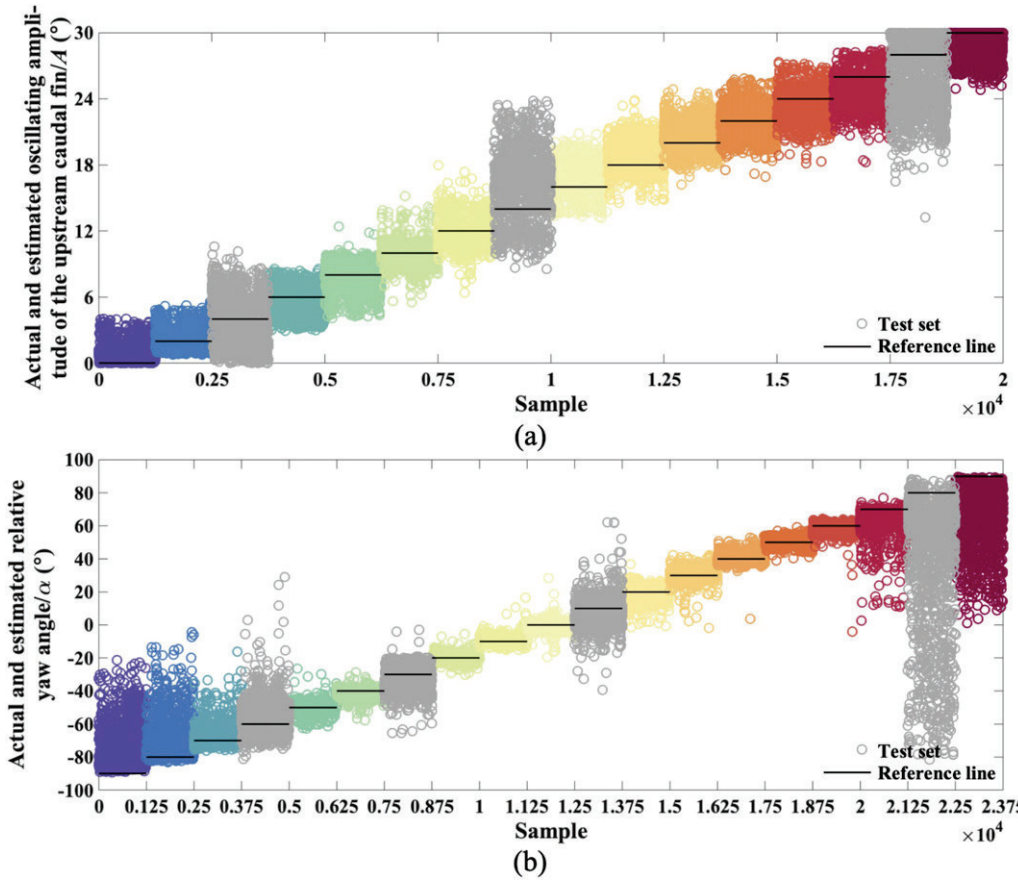

Figure 16. Results of RF-based relative yaw angle and oscillating amplitude estimation. (a) Oscillating amplitude estimation ($M_r = 1$, the pressure sensor used is P_0). (b) Relative yaw angle estimation ($M_r = 7$, the pressure sensors used are P_0, P_{L_1}, P_{R_1}, P_{R_2}, P_{L_2}, P_{L_4}, and P_{R_3}). In each subfigure, the different colors indicate the estimations for specific values of the relative states. The gray points mean the estimations of test set.

oscillating fin and the downstream robotic fish has been fixed at 10 cm in [21].

Such a relative longitudinal distance is relatively small when compared with the size of the robot. So the downstream robotic fish is not just a passive observer, but it actively changes the vortex wake generated by the upstream oscillating caudal fin. Figure 18 shows the instantaneous vortex structure by Q-criterion around the robotic fish body and HPVs on the surface of the robotic fish body. They are obtained by the computational fluid dynamics simulation software called Fluent. More details about the Fluent based simulation can be found in [21]. As shown in figure 18, the vortices disperse after they propagate over the fish head. As a result, the HPVs measured by the pressure sensors at the posterior of the downstream robotic fish have small variations.

4.2. The differences between investigating the relative yaw angle between the upstream oscillating fin and the downstream robotic fish and investigating the oscillating offset of the upstream oscillating caudal fin

The differences include three parts, such as the following:

First, in the experiments, the upstream oscillating caudal fin and the downstream robotic fish played roles as 'vortex signal generating source' and 'vortex signal detector', respectively. So, the difference between investigating the relative yaw angle of the downstream robotic fish and investigating the oscillating offset of the upstream oscillating caudal fin was the difference between changing the 'vortex signal generating source' and changing 'vortex signal detector'. Specifically, in the experiment of investigating the oscillating offset, the nonzero oscillating offset resulted in the deviation of the shedding vortices' propagating direction from the direction of the flow. Meanwhile, the scope of the backward reaction also deviated from the robotic fish in the downstream region. However, the downstream robotic fish that served the function of signal detector never changed. In the experiment of investigating the relative yaw angle, the pressure sensors mounted on the downstream robotic fish who served the function of hydrodynamic signal detector changed its orientation to the incoming flow as its attitude changed. Meanwhile, the body of the robotic fish may also cause flow separation [37] around itself and resulted in the self-generating vortices [38]. However, the upstream

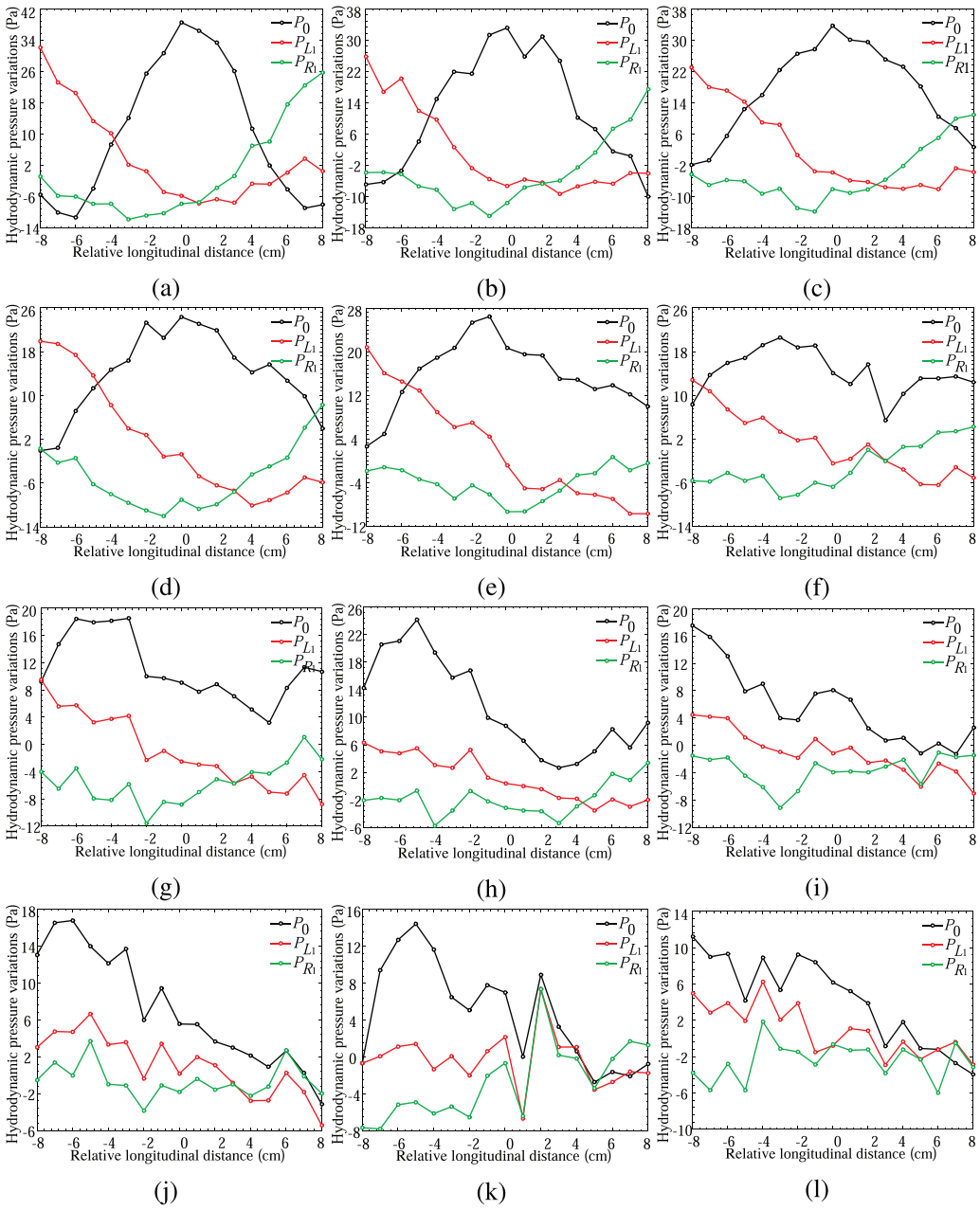

Figure 17. Hydrodynamic pressure variation with respect to the relative lateral distance d_{lateral} under different relative longitudinal distances $d_{\text{longitudinal}}$. (a) $d_{\text{longitudinal}} = 4$ cm, (b) $d_{\text{longitudinal}} = 6$ cm, (c) $d_{\text{longitudinal}} = 8$ cm, (d) $d_{\text{longitudinal}} = 10$ cm, (e) $d_{\text{longitudinal}} = 12$ cm, (f) $d_{\text{longitudinal}} = 14$ cm, (g) $d_{\text{longitudinal}} = 16$ cm, (h) $d_{\text{longitudinal}} = 18$ cm, (i) $d_{\text{longitudinal}} = 20$ cm, (j) $d_{\text{longitudinal}} = 22$ cm, (k) $d_{\text{longitudinal}} = 24$ cm, (l) $d_{\text{longitudinal}} = 26$ cm.

oscillating caudal fin who served as the hydrodynamic signal generating source never changed.

Second, in the experiment of investigating the oscillating offset of the upstream oscillating caudal fin, because the shedding vortices' propagating direction deviated from the direction of the flow, the vortex wake generated by the oscillating caudal fin may be dispersed by the flow. Thus it may be not as well-formed and stable as the vortex wake generated in the experiment of investigating the relative yaw angle.

Third, for the experiment of investigating the oscillating offset of the upstream oscillating caudal fin, the hydrodynamic pressure-bearing area of the downstream robotic fish was concentrated on the head of its body. Moreover, with the increasing oscillating offset, the above-mentioned area gradually decreased. This may result from the deviation of the vortex wake, as described in the second point. By comparison, the hydrodynamic pressure-bearing area can be almost distributed on the whole body of the robot with the changing orientation of the robot to the incoming flow in the experiment of investigating the relative yaw angle. The above-mentioned differences have resulted in the different qualitative and quantitative regularities of HPVs with respect to the experimental parameters. Specifically, in the experiment of investigating the oscillating offset, the HPVs measured by P_0, P_{L_1} and P_{R_1} change apparently with the

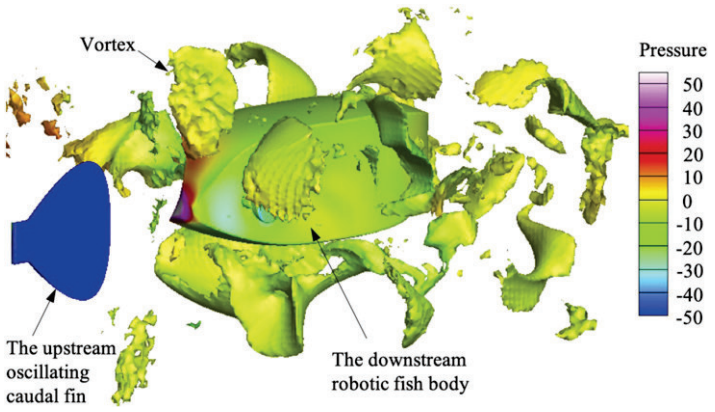

Figure 18. Instantaneous vortex structure by Q-criterion around the robotic fish body and HPVs on the surface of the robotic fish body. The animation of the vortices can be found in supplemental video.

oscillating offsets, whereas the changes of the HPVs measured by other pressure sensors are not apparent with the changing oscillating offsets. By comparison, in the experiment of investigating the relative yaw angle, the HPVs measured by all the pressure sensors have apparent changes with the changing relative yaw angles.

5. Conclusions and future work

This article has investigated the regression model, which links the ALLS-measured HPVs to the relative states between an upstream oscillating fin and a downstream robotic fish with leader–follower formation in a flume. Two criteria are proposed firstly for investigating not only the sensitivity of each pressure sensor to the variations of relative state variations, but also the insufficiency and redundancy of the pressure sensors used for regression analysis. Then four methods, including RF algorithm, BPNN, SVR, and REG, are used for establishing the regression model. Comparisons of the effects of the regression effects of using the four methods have been conducted, for determining the best method. The results show that the RF algorithm has the best excellent performance in estimating the relative states using the ALLS-measured HPVs. And RF-based regression models have been established for predicting the relative yaw angle and the oscillating amplitude of the upstream fin with small errors. Moreover, a further discussion for the flume experiments has been conducted in detail.

For different underwater vehicles like propeller-actuated autonomous underwater vehicle and ROV, the flow variations caused by the propeller and vehicle motions are essentially different from fin-actuated robot. In this article, we have selected a specifically designed mechatronic system (robotic fish) for investigating artificial lateral line system based relative state estimation. The regression methods used in this article could be used in other underwater mechatronic systems.

In the future, we will conduct an online estimation of the relative states between two adjacent freely-swimming robotic fish using the RF-based regression model. Free motions of the robotic fish result in rhythmical oscillations of the fish body, which may have significant effects on the ALLS-measured HPVs [39]. So the qualitative and quantitative relationships between the HPVs and the relative states may significantly differ from those we have investigated in this article and [21, 25]. Relative state estimation for two adjacent freely-swimming robotic fish would be more challenging.

Acknowledgments

This work was supported in part by Grants from the National Natural Science Foundation of China (NSFC, No. 91648120, 61633002, 51575005) and the Beijing Natural Science Foundation (No. 4192026). Liang Li acknowledges the Deutsche Forschungsgemeinschaft (DFG, German Research Foundation) under Germany's Excellence Strategy-EXC 2117-422037984, Zukunftskolleg Independent Research Grant (Grant No. P82967018 FP 330 670/18), the Max Planck Society, great support from Couzin lab, and the support of NVIDIA corporation with the donation of a Titan Xp.

ORCID iDs

Wei Wang https://orcid.org/0000-0003-4023-2845

References

[1] Bleckmann H 1986 *Role of the lateral line in fish behaviour* (Berlin: Springer)

[2] Chin C S and Lin W P 2018 Robust genetic algorithm and fuzzy inference mechanism embedded in a sliding-mode controller for an uncertain underwater robot *IEEE/ASME Trans. Mechatronics* **23** 655–66

[3] Gu N, Peng Z, Wang D, Shi Y and Wang T 2019 Antidisturbance coordinated path following control of

robotic autonomous surface vehicles: theory and experiment *IEEE/ASME Trans. Mechatronics* **24** 2386–96
[4] Wang N and Pan X 2019 Path following of autonomous underactuated ships: a translation-rotation cascade control approach *IEEE/ASME Trans. Mechatronics* **24** 2583–93
[5] Yu J, Wu Z, Su Z, Wang T and Qi S 2019 Motion control strategies for a repetitive leaping robotic dolphin *IEEE/ASME Trans. Mechatronics* **24** 913–23
[6] Ahrari A, Lei H, Sharif M A, Deb K and Tan X 2017 Reliable underwater dipole source characterization in 3D space by an optimally designed artificial lateral line system *Bioinsp. Biomim.* **12** 036010
[7] Ji M, Zhang Y, Zheng X, Lin X, Liu G and Qiu J 2018 Resolution improvement of dipole source localization for artificial lateral lines based on multiple signal classification *Bioinsp. Biomim.* **14** 016016
[8] Abdulsadda A T and Tan X 2013 Underwater tracking of a moving dipole source using an artificial lateral line: algorithm and experimental validation with ionic polymer-metal composite flow sensors *Smart Mater. Struct.* **22** 045010
[9] Ji M, Zhang Y, Zheng X, Lin X, Liu G and Qiu Q 2019 Performance evaluation and analysis for dipole source localization with lateral line sensor arrays *Meas. Sci. Technol.* **30** 115107
[10] Boulogne L H, Wolf B J, Wiering M A and van Netten S M 2017 Performance of neural networks for localizing moving objects with an artificial lateral line *Bioinsp. Biomim.* **12** 056009
[11] Wolf B J, Morton J A S, Macpherson W N and van Netten S M 2018 Bio-inspired all-optical artificial neuromast for 2d flow sensing *Bioinsp. Biomim.* **13** 026013
[12] Kanhere E, Wang N, Kottapalli A G P, Asadnia M, Subramaniam V, Miao J and Triantafyllou M 2016 Crocodile-inspired dome-shaped pressure receptors for passive hydrodynamic sensing *Bioinsp. Biomim.* **11** 056007
[13] Chen K, Tuhtan J A, Fuentes-Pérez J F, Toming G, Musall M, Strokina N, Kämäräinen J-K and Kruusmaa M 2017 Estimation of flow turbulence metrics with a lateral line probe and regression *IEEE Trans. Instrum. Meas.* **66** 651–60
[14] Kruusmaa M *et al* 2014 Filose for svenning: a flow sensing bioinspired robot *IEEE Robot. Autom. Mag.* **21** 51–62
[15] Lagor F D, Devries L D, Waychoff K M and Paley D A 2013 Bio-inspired flow sensing and control: autonomous rheotaxis using distributed pressure measurements *J. Unmanned Sys. Technol.* **1** 78–88
[16] Zhang F, Lagor F D, Yeo D, Washington P and Paley D A 2015 Distributed flow sensing for closed-loop speed control of a flexible fish robot *Bioinsp. Biomim.* **10** 065001
[17] Free B A and Paley D A 2018 Model-based observer and feedback control design for a rigid Joukowski foil in a Kármán vortex street *Bioinsp. Biomim.* **13** 035001
[18] Asadnia M, Kottapalli A G P, Haghighi R, Cloitre A, Alvarado P V. y., Miao J and Triantafyllou M 2015 Mems sensors for assessing flow-related control of an underwater biomimetic robotic stingray *Bioinsp. Biomim.* **10** 036008
[19] Yen W-K, Sierra D M and Guo J 2018 Controlling a robotic fish to swim along a wall using hydrodynamic pressure feedback *IEEE J. Oceanic Eng.* **43** 369–80
[20] Yen W-K and Guo J 2018 Phase controller for a robotic fish to follow an oscillating source *Ocean Eng.* **161** 77–87
[21] Zheng X, Wang C, Fan R and Xie G 2018 Artificial lateral line based local sensing between two adjacent robotic fish *Bioinsp. Biomim.* **13** 016002
[22] Asadnia M, Kottapalli A G P, Shen Z, Miao J and Triantafyllou M 2013 Flexible and surface-mountable piezoelectric sensor arrays for underwater sensing in marine vehicles *IEEE Sensor. J.* **13** 3918–25
[23] Dusek J, Kottapalli A G P, Woo M E, Asadnia M, Miao J, Lang J H and Triantafyllou M S 2013 Development and testing of bio-inspired microelectromechanical pressure sensor arrays for increased situational awareness for marine vehicles *Smart Mater. Struct.* **22** 014002
[24] Zheng X, Wang W, Xiong M and Xie G 2020 Online state estimation of a fin-actuated underwater robot using artificial lateral line system *IEEE Trans. Robot.* **36** 472–87
[25] Wang W, Zhang X, Zhao J and Xie G 2015 Sensing the neighboring robot by the artificial lateral line of a bio-inspired robotic fish *Proc. IEEE/RSJ Int. Conf. Intelligent Robots and Systems* (Hamburg, Germany) pp 1565–70
[26] Franosch J M P, Hagedorn H J, Goulet J, Engelmann J and van Hemmen J L 2009 Wake tracking and the detection of vortex rings by the canal lateral line of fish *Phys. Rev. Lett.* **103** 078102
[27] Ren Z and Mohseni K 2012 A model of the lateral line of fish for vortex sensing *Bioinsp. Biomim.* **7** 036016
[28] Akanyeti O, Venturelli R, Visentin F, Chambers L, Megill W M and Fiorini P 2011 What information do Kármán streets offer to flow sensing? *Bioinsp. Biomim.* **6** 036001
[29] Zheng X, Xiong M and Xie G 2019 Data-driven modeling for superficial hydrodynamic pressure variations of two swimming robotic fish with leader-follower formation *2019 IEEE Int. Conf. on Systems, Man and Cybernetics (SMC)* (IEEE) pp 4331–6
[30] Abdulsadda A T and Tan X 2013 Nonlinear estimation-based dipole source localization for artificial lateral line systems *Bioinsp. Biomim.* **8** 026005
[31] DeVries L and Paley D A 2013 Observability-based optimization for flow sensing and control of an underwater vehicle in a uniform flowfield *2013 American Control Conf.* (IEEE) pp 1386–91
[32] Breiman L 2001 Random forests *Mach. Learn.* **45** 5–32
[33] Liu Y, Wang Y and Zhang J 2012 New machine learning algorithm: random forest *Int. Conf. on Information Computing and Applications* (Springer) 246–52
[34] Hsu K-l., Gupta H V and Sorooshian S 1995 Artificial neural network modeling of the rainfall-runoff process *Water Resour. Res.* **31** 2517–30
[35] Hecht-Nielsen R 1992 Theory of the backpropagation neural network *Neural Networks for Perception* (Amsterdam: Elsevier) pp 65–93
[36] Gunn S R *et al* 1998 Support vector machines for classification and regression *ISIS Technical Report* **14** 5–16
[37] Anderson J D Jr 2010 *Fundamentals of Aerodynamics* (New York: McGraw-Hill)
[38] Kodati P and Deng X 2006 Towards the body shape design of a hydrodynamically stable robotic boxfish *Proc. IEEE Int. Conf. on Robotics and Automation* (Beijing, China) pp 5412–7
[39] Zheng X, Wang M, Zheng J, Tian R, Xiong M and Xie G 2019 Artificial lateral line based longitudinal separation sensing for two swimming robotic fish with leader-follower formation *2019 IEEE/RSJ Int. Conf. on Intelligent Robots and Systems (IROS)* (IEEE) pp 2539–44